

UNIVERSITI MALAYSIA PAHANG

DECLARATION OF THESIS / UNDERGRADUATE PROJECT PAPER AND COPYRIGHT

Author's full name : NURWAHIDAH BINTI MARIZAN

Date of birth : 2<sup>ND</sup> FEBRUARY 1985

Title : DEVELOPMENT OF  $\text{La}_{(1-x)}\text{Fe}_x\text{Mn}$  OXIDE OF HYDROGEN  
STORAGE FOR OF FUELL CELL APPLICATION.

Academic Session : 2007/2008


I declare that this thesis is classified as:

- CONFIDENTIAL** (Contains confidential information under the Official Secret Act 1972)\*
- RESTRICTED** (Contains restricted information as specified by the organization where research was done)\*
- OPEN ACCESS** I agree that my thesis to be published as online open access (full text)

I acknowledged that University Malaysia Pahang reserves the right as follows:

1. The thesis is the property of University Malaysia Pahang.
2. The Library of University Malaysia Pahang has the right to make copies for the purpose of research only.
3. The Library has the right to make copies of the thesis for academic exchange.

  
\_\_\_\_\_  
SIGNATURE

Certified by:  
  
\_\_\_\_\_  
(SIGNATURE OF SUPERVISOR)

850202-08-6246  
(NEW IC NO./PASSPORT NO.)

MR. SYAMSUL BAHARI BIN ABDULLAH  
NAME OF SUPERVISOR

Date : 28 APRIL 2008

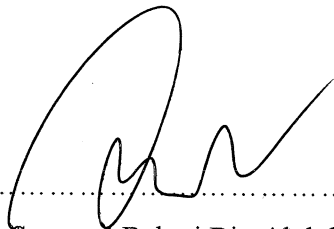
Date : 28 APRIL 2008



If the thesis is CONFIDENTIAL or RESTRICTED, please attach with the letter from the organization with period and reasons for confidentiality or restriction.

I hereby declare that I have read this thesis  
and in my opinion this thesis is sufficient in terms of scope and quality for the  
award of the degree of Bachelor of Chemical Engineering (Gas technology)

Signature



.....

Name of Supervisor : Mr. Syamsul Bahari Bin Abdullah

Date : 28<sup>th</sup> April 2008

**DEVELOPMENT OF  $\text{La}_{1-x}\text{Fe}_x\text{Mn}$  OXIDE OF HYDROGEN STORAGE FOR  
FUEL CELL APPLICATION.**

**NURWAHIDAH MARIZAN**

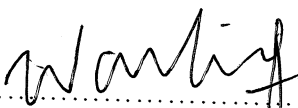
**A report submitted in partial fulfillment of the requirements for the award of  
the degree of bachelor of chemical engineering (gas technology)**

**Faculty of Chemical Engineering & Natural Resources  
Universiti Malaysia Pahang**

**APRIL 2008**

PERPUSTAKAAN UNIVERSITI MALAYSIA PAHANG	
No. Perolehan <b>031417</b>	No. Panggilan TP 156 A35 N87 2008 rs Thesis
Tarikh <b>11 JUL 2008</b>	

I declare that this thesis entitled "Development of  $\text{La}_{1-x}\text{Fe}_x\text{Mn}$  oxide of hydrogen storage for fuel cell application." is the results of my own research except as cited in the references. This thesis has not been accepted for any degree and is not concurrently submitted in candidature of any other degree.

Signature :  .....

Name : Nurwahidah Binti Marizan

Date : 28<sup>th</sup> April 2008

## ACKNOWLEDGEMENT

In preparing this thesis, I was in contact with many people, researchers, academicians, and practitioners. They have contributed towards my understanding and thoughts. In particular, I wish to express my sincere appreciation to my main thesis supervisor, Mr. Syamsul Bahari Bin Abdullah, for encouragement, guidance, critics and friendship. I am also very thankful to Head of Gas Department Mr. Arman Abdullah and PJP Mr. Khairul Nizam for their guidance, advices, help and motivation. Without their continued support and interest, this thesis would not have been the same as presented here.

I am also indebted to University Malaysia Pahang (UMP) for supplying all the facilities to have relevant literatures.

My fellow postgraduate students should also be recognized for their support. My sincere appreciation also extends to all my colleagues and others who have provided assistance at various occasions. Their views and tips are useful indeed. Unfortunately, it is not possible to list all of them in this limited space. I am grateful to all my family members.

## ABSTRACT

The development and characteristic of  $\text{La}_{(1-x)}\text{Fe}_x\text{Mn}$  oxide in storing hydrogen gas examined in this study. The adsorption capacity of La based alloy was monitored under the influence of mole fraction(x) which is  $x = 0.05, 0.1$  and  $0.2$ . Due to the limitation on its operating conditions, the pressure chosen was 2 bar while the temperature was  $100^\circ\text{C}$  in 1 hour experimental time. The alloy was process using sintering process pada suhu  $550^\circ\text{C}$ . Scanning electron microscopy (SEM) showed the microstructure of the La based alloy after the sintering process with the different of mole fraction in each samples. The thermal stability of the alloy was examined using thermal gravimetric analysis (TGA) apparatus. The Fourier Transform Infra Red (FTIR) was used to detect whether the hydrogenation process was occur in the alloy. The results of this study showed that adsorption process occur as well as oxidation process during the hydrogenation process. The smallest mole fraction(x) which is  $x = 0.05$  showed the highest weight loss during the hydrogenation process. The adsorption of hydrogen in the alloy oxide was proved by FTIR using the detection of the wavelength in the range of  $760\text{ cm}^{-1}$  based on the previous research done by Fujimori et al.

## ABSTRAK

Permbentukan dan cirri-ciri  $\text{La}_{(1-x)}\text{Fe}_x\text{Mn}$  oksida dalam penyimpanan gas hydrogen telah dilakukan dalam penyelidikan ini. Keupayaan alloy beraskan lanthanum ini dipengaruhi oleh pecahan mol(x) dimana  $x = 0.05, 0.1$  dan  $0.2$ . Experimen dijalankan pada tekanan 2 bar dan suhu pada  $100^\circ\text{C}$  selama 1 jam. Alloy di fabrikasi menggunakan process sintering pada suhu  $500^\circ\text{C}$ . Analisis SEM dijalankan selepas proses sintering dilakukan bagi pecahan mole yang berlainan. Kestabilan thermal dikaji menggunakan TGA bagi mengetahui kadar penurunan berat semasa proses sintering. Analisis menggunakan FTIR dilakukan bg mengetahui sama ada proses hydrogenasi berlaku atau pun sebaliknya. Berdasarkan uji kaji selain proses hydrogenasi, terdapat juga berlakunya proses penurunan berdasarkan pengurangan berat alloy selepas uji kaji. Bilangan pecahan mol yang terkecil iaitu  $x = 0.05$  menunjukkan kadar pengurangan berat yang palaing banyak. Penyerapan hydrogen dalam alloy oksida dibuktikan menggunakan FTIR dengan julat jarak gelombang  $760\text{ cm}^{-1}$  berdasarkan kajian sebelum ini oleh Fujimori et al.

**TABLE OF CONTENT**

<b>CHAPTER</b>	<b>TITLE</b>	<b>PAGE</b>
	<b>DECLARATION</b>	<b>ii</b>
	<b>DEDICATION</b>	<b>iii</b>
	<b>ACKNOWLEDGEMENT</b>	<b>iv</b>
	<b>ABSTRACT</b>	<b>v</b>
	<b>ABSTRAK</b>	<b>vi</b>
	<b>TABLE OF CONTENTS</b>	<b>vii</b>
	<b>LIST OF TABLES</b>	<b>x</b>
	<b>LIST OF FIGURES</b>	<b>xi</b>
	<b>LIST OF SYMBOLS</b>	<b>xii</b>
	<b>LIST OF APPENDICES</b>	<b>xiii</b>
<b>1</b>	<b>INTRODUCTION</b>	
	1.1 General	1
	1.2 Problem Statement	2
	1.3 Objective	2
	1.4 Scope of Research	2
	1.5 Current research	3
<b>2</b>	<b>LITERITURE REVIEW</b>	
	2.1 General	4
	2.2 Reduction Process	5
	2.3 Characterization	10



2.4	Alloy fabrication by Melting Process	12
2.5	Alloy Fabrication by Ball Milling	15
2.6	Mechanical Alloying	17
2.7	Scanning Electron Microscopy (SEM)	17
2.8	Thermal Gravimetric Analysis (TGA)	18
2.9	Fourier Transform Infra Red (FTIR)	19
2.10	Summary	19

### **3 MATERIALS & METHOD**

3.1	Materials & Apparatus	23
3.2	Equipment	23
3.3	Preparation	
3.3.1	La based alloy	23
3.3.2	Rig	24
3.4	Analysis before Experiment	24
3.5	Running the Experiment	
3.5.1	General Procedure for Rig Operation	25
3.5.2	Details procedure of Hydrogenation Process	
a.	Safety & Leakage Testing	25
b.	Operating Procedure for Alloy Activation Process	25
c.	Hydrogenation Process	26
3.6	Data Collecting	
3.6.1	Alloy Mixing	27
3.6.2	Adsorption Performance	27
3.6.3	Fourier Transform Infra Red (FTIR)	27
3.7	Analyzing data	
3.7.1	Microstructure of Alloy	28
3.7.2	TGA Analysis	28
3.7.3	FTIR Analysis	28

3.7.4	Adsorption Performance	28
<b>4</b>	<b>RESULTS &amp; DISCUSSION</b>	
4.1	Alloy fabrication	30
4.2	Characterizations	
4.2.1	Scanning Electron Microscopy (SEM)	31
4.2.2	Thermalgravimetris Analysis (TGA)	33
4.2.3	Fuorier Transform Infra Red (FTIR)	35
4.3	Reduction percentage	37
<b>5.</b>	<b>CONCLUSIONS &amp; RECOMENDATIONS</b>	<b>38</b>
<b>6.</b>	<b>REFERENCES</b>	<b>40</b>
	<b>Appendices A-D</b>	<b>42</b>

**LIST OF TABLES**

<b>TABLE NO.</b>	<b>TABLE</b>	<b>PAGE</b>
1	Summary of methods and materials of previous researcher.	11
2	Observation During the Mixing Process.	21
3	Weight loss percentage / temperature	33
4	Position of FTIR bands of lanthanum hydrides according to the present work and the literature	35
5	Percentage of reduction ( $\text{La}_{1-x}\text{Fe}_x\text{Mn}$ ) oxide in operating condition at $P= 2\text{bar}$ , $T= 100^\circ\text{C}$ and $t = 1 \text{ hr}$ .	36

## LIST OF FIGURES

FIGURE NO.	TITLE	PAGE
1	Reduction curves of MnO <sub>2</sub> at 1275C in H <sub>2</sub> , He and Ar	8
2	Methodology	21
3	Test rig for the experiment	23
4	Test Rig for Hydrogenation Process	28
5	SEM image of (La <sub>1-x</sub> Fe <sub>x</sub> Mn) oxide, x=0.05	30
6	SEM image of (La <sub>1-x</sub> Fe <sub>x</sub> Mn) oxide, x=0.1	31
7	SEM image of (La <sub>1-x</sub> Fe <sub>x</sub> Mn) oxide, x=0.2	31
8	TGA curve of (La <sub>1-x</sub> Fe <sub>x</sub> Mn) oxide, x=0.05	32
9	TGA curve of (La <sub>1-x</sub> Fe <sub>x</sub> Mn) oxide, x=0.1	32
10	TGA curve of (La <sub>1-x</sub> Fe <sub>x</sub> Mn) oxide, x=0.2	33
11	Spectrum of (La <sub>1-x</sub> Fe <sub>x</sub> Mn) oxide, x=0.05 after hydriding process	34
12	Spectrum of (La <sub>1-x</sub> Fe <sub>x</sub> Mn) oxide, x=0.1 after hydriding process	34
13	Spectrum of (La <sub>1-x</sub> Fe <sub>x</sub> Mn) oxide, x=0.2 after hydriding process	35
14	Hydrogenation Test Rig	46
15	Reservoir & Reactor of the Hydrogenation Test Rig.	46
16	Tangent of TGA Curve.	47

**LIST OF SYMBOL**

P	-	Pressure
%	-	Percent
T	-	Temperature
m	-	Mass
MW	-	Molecular weight
°	-	Degree
rpm	-	Radius per hour
PG	-	Pressure gauge
V	-	Valve
K	-	Kelvin
H	-	hydrogen
M	-	Metal
t	-	Time
BSE	-	Back Scatred electron

**LIST OF APPENDICES**

<b>APPENDIX NO.</b>	<b>TITLE</b>	<b>PAGE</b>
A	Mol & Mass Calculation for Alloy compounds	43 - 44
B	Table for Hydrogenation data	45
C	Hydrogenation Test Rig	46
D	Tangent Line of TGA Curve	47

## CHAPTER 1

### INTRODUCTION

#### 1.1 General

The pollution from motor cars is particularly in city areas, becoming increasingly unacceptable to people living in, visiting or working in the cities of the world. Demands for zero-emission vehicles have been voiced, and the automobile industry is facing louder criticism for not addressing the problem. Hydrogen is the most promising candidate to replace the current fossil. One of the prerequisites for the utilization of hydrogen as fuel in car engines or aircraft turbines is a device for the safe and easily handled storage and transportation of hydrogen.

Several methods have been proposed for this purpose. Among them are high-pressure tanks for gaseous hydrogen, cryogenic vessels for liquid hydrogen and metal hydride storage systems. However, the first two options bear the danger of explosion if improperly handled, and the latter method suffers from high cost and weight. As an alternative, one could envisage hydrogen storage by encapsulation in micro porous media. Thus, the working principle is that the guest molecules are forced, under elevated temperatures and pressures, into the cavities of the molecular sieve host. Upon cooling to room temperature or below, hydrogen is trapped inside the cavities. It can be released again by raising the temperature. The form of hydrogen storage most suitable depends on the application.

## 1.2 Problem Statement

Applications in the transportation sector require storage at a volume that can be accommodated within the vehicles and at a weight that does not limit the performance of the vehicles. A well known case is the detrimental influence on the development and used hydrogen in the transportation industry caused by the Hindenburg accident in 1936. The approach to handling safety issue for hydrogen applications in the energy sector, affecting society broadly in a number of different ways, requires a way of handling the unanticipated safety related events bound to occur in a technology that is significantly different from that currently used. All components of hydrogen systems for vehicles must be assessed for safety under the conditions of both normal operation and accidents involving collisions between the car and other stationary or moving object. To be accepted by the public as a transportation fuel, hydrogen needs to be accessible and easily stored onboard an automobile in suitable quantities.

## 1.3 Objective

Through out this research, the objectives are:

- i. To fabricate La based alloy for hydrogen storage.
- ii. To study the characterizations and the effect of different base fraction in alloy during hydrogenation.

## 1.4 Scope of Research

Based on the literature, scopes of research are:

- i. The characterization of  $\text{La}_{1-x}\text{Fe}_x\text{Mn}$  oxide of hydrogen storage using SEM, FTIR and TGA.
- ii. To study the impact of using metal oxide as hydrogen storage.



## 1.5 Current Research

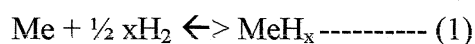
The purpose of this research is to study the impact of using metal oxide as hydrogen storage alloy. The influence of mole fraction ( $x$ ) is a parameter in this study. The different value of ( $x$ ) plays an important role that influences the adsorption of hydrogen in the alloy oxide. The hydrogenation test rig was fabricated to test the adsorption capacity of the alloy. The operating conditions for this study are set by the pressure of 2 bar and the temperature of 100°C.

## CHAPTER 2

### LITERATURE REVIEW

#### 2.1 General

Most scientists working on the problem are focusing on storing the gas in solids and solid matrices--forms in which it's possible to exceed the density of liquid hydrogen. Storing hydrogen in hydrides, carbon-based materials, hydrogen-containing compounds, and other solids offers a number of potential advantages over other storage methods [1]. Metal hydride is when metal alloys are combined with hydrogen can be absorb and store hydrogen within the structure. This is how metal hydride work during the adsorption process to store hydrogen. In the grain there are two phases which are matrix and second phase. The matrix divided into two which are metal and hydride. The metal will become charging and the hydride becomes the discharging. In the second phase the metal will be discharging and the hydride will be charging. The hydrogenation processes occur like this. First, hydrogen molecules land on the surface, disassociated and get absorbed. Then, hydrogen atom dissolves and diffuses into matrix. The lattice will expend. As the hydrogen metal ratio increase, the strong H-H bond interactions take place and the hydride phase. The general equation of metal hydride formation is



Where Me stand for metal or metal alloy, such  $A_mB_n$  or higher order alloy. Binary and higher metal alloys generally store similar amounts of hydrogen by volume, but less hydrogen by mass. The hydride of the composition  $\text{MgH}_2$  seems the most interesting

single metal hydride, with its fairly high hydrogen fraction of 7.6% by mass. Although, desorption temperature is higher than ambient temperature, it could be made available in motorcars, although this would lower the overall efficiency. The kinetic restraints at near ambient pressures make the absorption and desorption processes very slow, and desorption times in the range of hours and unacceptable, at least for mobile applications. Other binary hydrides can be formed with light elements, without improvement in performances. For heavy metal, only palladium has received some attention, due to rapid absorption and desorption at ambient temperature and pressure. However, only 0.6% hydrogen by mass is stored, which high metal cost makes this option unattractive.

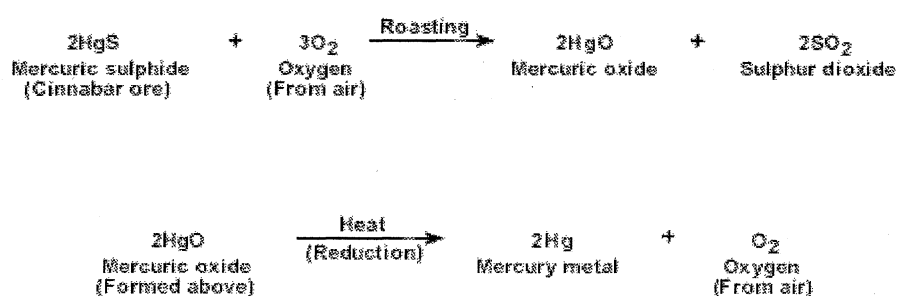
Hydrides with two metal constituents studied include a range of Mg alloys, including interesting ones with Ni and Fe, as well as alloys containing Al, Fe, Ni, Ti, and La, as well as other metals. Of the total number of atoms, say  $6 \times 10^{28}$  per  $\text{m}^3$ , the hydrogen fraction usually below the value of 2 for  $\text{MgH}_2$ . The mass fraction achieved for these hydrides is often below 2%, with the  $\text{LaNi}_5\text{H}_7$  [1]. Its volumetric density is about  $115 \text{ kg H}_2$  per  $\text{m}^3$ , and the enthalpy evolution during absorption is  $-30.8 \text{ kg mol}^{-1}$ . While the maximum numbers of hydrogen atoms that can be accommodated within in the  $\text{LaNi}_5$ , sometimes only 6 are incorporated, possibly due to the swelling of those unit cells that already has accepted 7 H atoms [1]. Based on theory lanthanum capable to storing up to 400 times their own volume of hydrogen gas in a reversible adsorption process. One of the advantage of using lanthanum as a based alloy is because desorption slightly near 1 bar [2]. Among these materials, the  $\text{LaNi}_5$  alloy exhibits excellent hydrogen storage characteristics such as high volumetric storage density, easy activation, moderate plateau pressures and easy modulation of hydrogen storage properties by substituting different elemental species into the La or Ni lattice sites.

## 2.2 Reduction process

Reduction process is used for converting metal-oxides into metal. Metal-chloride can also be reduced directly. The reduction reaction chosen depends on the

chemical reaction or reactivity of metals. Generally reduction by heat, chemical reduction or electrolytic reduction processes are utilized.

- i. Reduction by heat: Metals that are unreactive, like Hg, can be reduced from their ores by heating them. Mercury ore cinnabar is actually mercury sulphide. This can be heated at  $300^{\circ}\text{C}$  so that S is removed as  $\text{SO}_2$  and  $\text{HgO}$  is obtained. Hg is a very unreactive metal.  $\text{HgO}$  dissociates into Hg and oxygen soon. The reaction is shown below.



It is interesting to note that for the cinnabar ore, roasting and reduction processes go on one after another.

- ii. Chemical reduction: Various reducing agents are used for different metal-oxides to obtain free metals. Carbon, Al, Na, Ca are some reducing agents that are put in use.

- a. Reduction by carbon: Oxides of Zn, Fe, Ni, Sn, Pb are reduced by heating them with carbon. Metal-oxide is mixed with coke, a source of carbon, and heated in a furnace. Carbon reacts with oxygen and free metal is obtained. Example below shows how Zn is obtained from  $\text{ZnO}$  on reduction with coke.



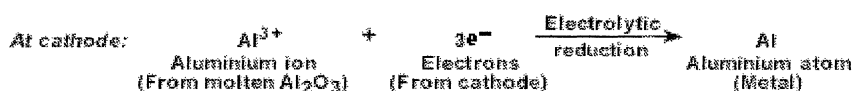
Reduction by carbon cannot be done for more reactive metals like Mn, Al, Cr, etc. Cu-oxide can be reduced by coke, but Ca-oxide cannot be reduced by coke.

- b. Reduction by Al: This process is called as the Thermite process. Al is more reactive than carbon. Some metal-oxides that cannot be reduced by coke are reduced by Al. Al itself attracts oxygen from the metal-oxide and becomes aluminium oxide, and this frees the metal. Mn and Cr metals oxides are extracted and reduced by Al. Example below shows what happens when manganese dioxide is heated with aluminium powder.

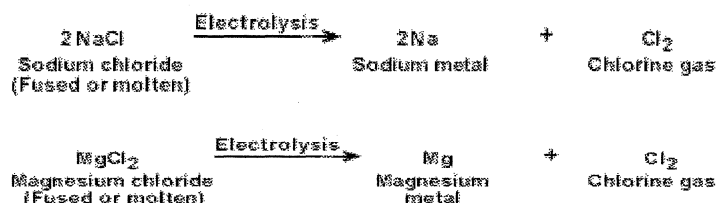


- c. Reduction by electrolysis: Highly reactive metal-oxides and metal-chlorides are not easy to be reduced by chemical reactions. Metals such as Na, K, Mn, Ca have to be freed from their ores by electrolytic processes. These metals are so reactive that they themselves are powerful reducing agents. Molten metal-oxides or chlorides form the electrolyte in the electrolytic cell. The cathode of the cell provides the electrons needed for the metal to free itself from the metal-oxide or metal-chloride bonds.

$\text{Al}_2\text{O}_3$  is reduced at the cathode of an electrolytic cell as shown below.  $\text{Al}_2\text{O}_3$  is melted and forms the electrolyte. Free  $\text{Al}^{3+}$  ions are attracted to the negatively charged cathode.  $\text{Al}^{3+}$  is reduced by supply of electrons at the cathode.

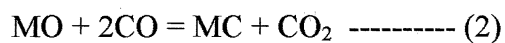


Chlorides of metals like Na, Mg are melted to form electrolytes. The reactions are shown below.



Chlorine gas is liberated at the anode. The electrolysis has been done with molten metal ores and not aqueous solutions because these metals are highly reactive and will react with water to give hydroxides and not pure metals. In the electrolysis, metals atoms get deposited on the cathode electrodes which then have to be carefully removed and stored [17].

Carbothermal reduction of stable metal oxides such as  $\text{MnO}$ ,  $\text{Cr}_2\text{O}_3$ ,  $\text{TiO}_2$  and  $\text{Al}_2\text{O}_3$  requires high temperatures. Obviously, to have high productivity, industrial processes are run at much higher temperatures than those listed in Table 1. At these temperatures, ores are liquid, and reduction occurs from molten slag, in which activity of an oxide is low, while carbon monoxide pressure at the reaction interface has to be above 1 atm to provide conditions for a gas bubble nucleation. Thus, ferromanganese is produced at about  $1500^\circ\text{C}$ ; temperature in the ferrochromium production is above  $1700^\circ\text{C}$ . Carbothermal reduction of titania to titanium carbide is also implemented at high temperatures,  $1700\text{--}2100^\circ\text{C}$ . High temperature for carbothermal reduction of alumina is a major obstacle in development of carbothermal technology for aluminium production. Needless to say that high temperature processes are energy demanding and have high maintenance cost. Production efficiency can be improved if the reduction temperature is lowered. This can be achieved by changing the equilibrium conditions and increasing the reduction rate. One way in this direction is to use methane-containing gas, which offers more favorable thermodynamics in comparison with solid carbonaceous materials. Reduction temperatures under standard conditions are much lower than in carbothermal reduction with solid carbon. In addition to thermodynamic advantage, the gas-solid reaction has a higher rate in comparison with solid-solid carbon-oxide reaction. Another way to decrease the temperature of carbothermal reduction of stable oxides is decreasing the CO partial pressure and/or increasing mass transfer in the gas phase. This can be achieved by running reduction processes in inert atmosphere or in hydrogen, which is also involved in the reduction reactions. It is well recognised that carbothermal reduction of metal oxides in the solid state goes through the gas phase. Reduction of oxide MO to carbide MC can be presented by Reactions (1) and (2):



In these reactions, carbon and oxygen are transferred between solid phases by CO and CO<sub>2</sub>, respectively. Gas phase also plays important role when reduction proceeds with formation of metal or metal oxide vapour, as in the case of alumina reduction. Gas species are directly involved in the carbothermal reactions; the composition of the gas phase may affect the reaction rate. This is illustrated by Figure 1 which presents reduction curves for manganese oxide obtained in hydrogen, helium and argon. Reduction is much faster in hydrogen than in helium, and faster in helium than in argon[16].

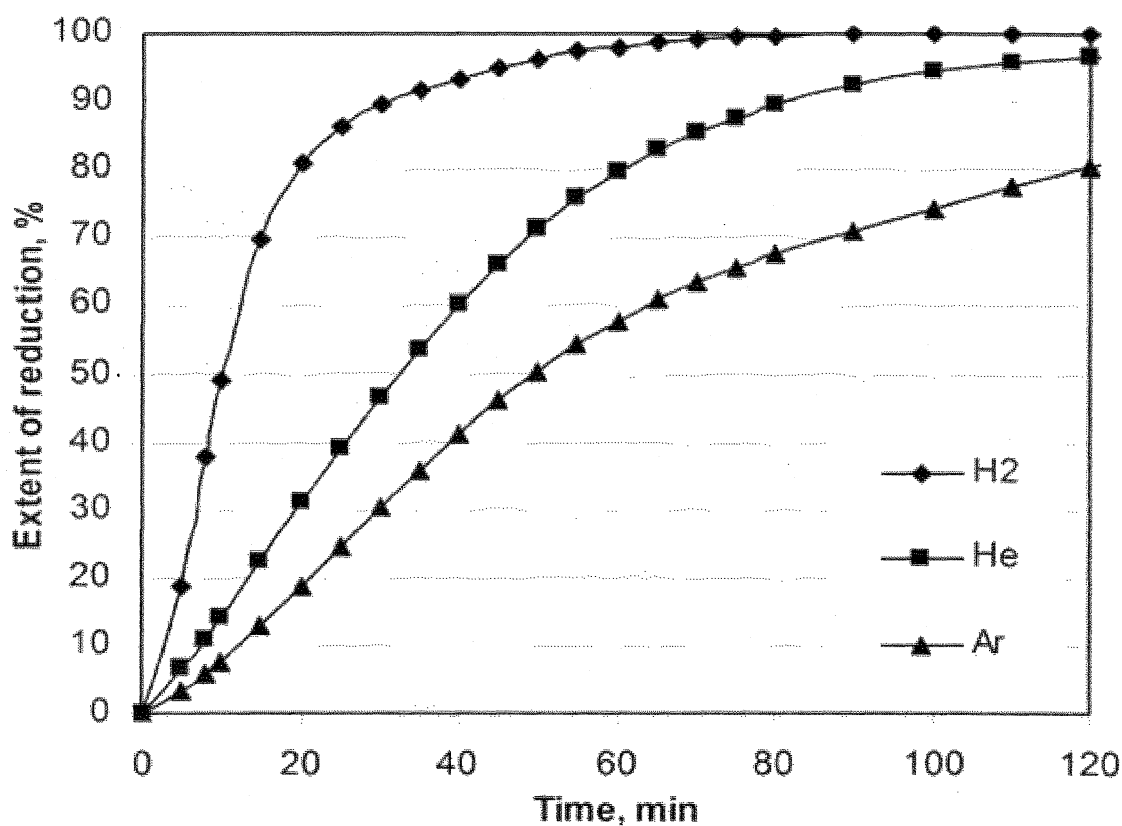


Figure 1 Reduction curves of MnO<sub>2</sub> at 1275C in H<sub>2</sub>, He and Ar

## 2.3 Characterization

### 2.3.1 Scanning Electron Microscopy (SEM)

Technique that which will forms an image of a microscopic region of the specimen surface. An electron beam from 5 to 10 nm in diameter is scanned across the specimen. The interaction electron beam with the specimen produces a series of phenomena such as:

- i. Backscattering of electrons of high energy
- ii. Secondary electrons of low energy
- iii. Absorption of electrons, measurable as specimen current
- iv. X-rays
- v. Visible light (cathodoluminescence)

Any one of these signals can be continuously monitored by detectors. The detector signal is amplified and used to modulate the brightness of a cathode ray tube, the beam of which is scanned in synchrony with the electron beam impinging upon the specimen. A correspondence between each scanned point at the specimen surface and a corresponding point on the cathode ray tube screen is thus established. The area scanned upon the specimen is very small in comparison with the corresponding area on the cathode ray tube screen. The magnification of the image on the screen is the ratio of a distance on the screen and the corresponding distance on the specimen. Due to the way these images are created, SEM micrographs have a very large depth of focus yielding a characteristic three-dimensional appearance useful for understanding the surface structure of a sample. This great depth of field and the wide range of magnifications (commonly from about 25 times to 250,000 times) are available in the most common imaging mode for specimens in the SEM, secondary electron imaging, such as the micrograph taken of pollen shown to the right. Characteristic x-rays are the second most common imaging mode for an SEM. X-rays are emitted when the electron beam removes an inner shell electron from the sample, causing a higher energy electron to fill the shell and give off energy. These characteristic x-rays are used to identify the elemental composition of the sample. Back-scattered electrons (BSE) that come from



the sample may also be used to form an image. BSE images are often used in analytical SEM along with the spectra made from the characteristic x-rays as clues to the elemental composition of the sample[21].

### 2.3.2 Thermal gravimetric analysis (TGA)

Thermogravimetric Analysis (TGA) measures the amount and rate of change in the weight of a material as a function of temperature or time in a controlled atmosphere. Measurements are used primarily to determine the composition of materials and to predict their thermal stability at temperatures up to 1000°C. The technique can characterize materials that exhibit weight loss or gain due to decomposition, oxidation, or dehydration. The TGA are used to measure:

- i. Thermal Stability of Materials
- ii. Oxidative Stability of Materials
- iii. Composition of Multi-component Systems
- iv. Estimated Lifetime of a Product
- v. Decomposition Kinetics of Materials
- vi. The Effect of Reactive or Corrosive Atmospheres  
on Materials
- vii. Moisture and Volatiles Content of Materials

There are 2 mechanism that occur which are weight loss or weight gain. Weight gain and weight loss happen due much process such as[21]:

- i. Weight Loss:
  - Decomposition: The breaking apart of chemical bonds.
  - Evaporation: The loss of volatiles with elevated temperature.
  - Reduction: Interaction of sample to a reducing atmosphere (hydrogen, ammonia, etc).

- Desorption.

ii. Weight Gain:

- Oxidation: Interaction of the sample with an oxidizing atmosphere.
- Absorption.

### 2.3.3 Fourier Transform Infra Red (FTIR)

FT-IR stands for Fourier Transform Infra Red, the preferred method of infrared spectroscopy. In infrared spectroscopy, IR radiation is passed through a sample. Some of the infrared radiation is absorbed by the sample and some of it is passed through (transmitted). The resulting spectrum represents the molecular absorption and transmission, creating a molecular fingerprint of the sample. Like a fingerprint no two unique molecular structures produce the same infrared spectrum. This makes infrared spectroscopy useful for several types of analysis. So, the information that can FT-IR provide are[21]:

- i. It can identify unknown materials
- ii. It can determine the quality or consistency of a sample
- iii. It can determine the amount of components in a mixture

## 2.4 Alloy Fabrication by Melting Process

Based on Shih et al. study, the  $\text{LaNi}_{4.25}\text{Co}_{0.5}\text{V}_{0.1}$  alloy was prepared by arc melting, followed by annealing at  $1100^{\circ}\text{C}$  under vacuum for 10h as report previously. It was then pulverized into a sieve of size smaller than  $44\mu\text{m}$  by repeated hydriding / dehydriding [3]. The alloy powder was mixed with Ag flakes ( $\sim 44\mu\text{m}$ ) or spherical Ni powder ( $25\mu\text{m}$ ) in different molar ratios, pressed at pressure of  $125\text{kg}/\text{cm}^2$  to form pallet of diameter 14mm and then sintered in vacuum at  $450$  or  $700^{\circ}\text{C}$  for 5h respectively. The process in which a mixture alloy is compressed at low pressure and then sintered to make a nonbreakable metal hydride alloy pallet is suitable for various hydrogen storage

alloys and metallic binders. If  $\text{LaNi}_{4.25}\text{Co}_{0.5}\text{V}_{0.1}$  is used, the composition of  $\text{Ag}/\text{AB}_5 = 10$  &  $\text{Ni}/\text{AB}_5 = 25$  can satisfy the condition that the pellets maintain integrity without breaking after repeated gas or electrochemical hydrogen absorption/desorption cycles. The volume expansion of the pellets  $\text{Ag}/\text{AB}_5 = 10$  and  $\text{Ni}/\text{AB}_5 = 25$  after hydrogenation are approximately 8% and 5% respectively. The number and size of the microholes in the pellet  $\text{Ni}/\text{AB}_5 = 25$  are larger than those in the pellet  $\text{Ag}/\text{AB}_5 = 10$ . The different shape of Ni powder and Ag flakes make the difference. This difference also affects the discharge capacity. So, that the pellet  $\text{Ni}/\text{AB}_5 = 10$ .

The  $\text{LaNi}_{4.25}\text{Al}_{0.75}$  alloy was prepared in a high frequency induction melting furnace using argon atmosphere protection [6]. The purities of starting materials were: La 99.5%, Ni 99.99% and Al 99.7%. The ingot was then annealed at 1323K for 8h in argon atmosphere in a sealed quartz tube. Based on Cheng et al. findings, long term cycling resulted in continued pulverization of the alloy.

$\text{LaNi}_{4.25}\text{Al}_{0.75}$  is supplied by Institute of Metal Research CAS, was prepared by vacuum melting of La and Ni component with subsequent addition of aluminium to the melt, and the composition was determined by method of chemical analysis [7].  $\text{LaNi}_{4.25}\text{Al}_{0.75}$  granules of <2mm in diameter were chosen as sample, which was taken from the interior of the alloy ingot. Tritium and deuterium gases are stored on uranium beds and delivered as needed. Based on the research,  $\text{LaNi}_{4.25}\text{Al}_{0.75}$  is easily activated. In addition, the absorption-desorption processing is rapid and does not need a long equilibrium time. It can be concluded that  $\text{LaNi}_{4.25}\text{Al}_{0.75}$  is a good material for hydrogen isotopes storage and pump over.

Based on Gao et al. method, the alloy sample was prepared by vacuum induction melting in an atmosphere of high purity argon [8]. The alloy ingot was mechanically pulverized into particles below 200 meshes in air. The sample powders were introduced into 100ml stainless steel vial together with stainless steel ball ( $d = 10\text{mm}$ ) on a QM-ISP planetary-type ball mill. The weight ratio of the ball to powder was 20:1. The vial was then evacuated, filled with high purity argon to 0.2-0.3 MPa and tightly sealed to avoid

contamination by air. The ball milling time was fixed at 350rpm. Based on the finding, mechanical ball milling under argon can improve the hydriding/dehydriding properties of  $\text{La}_{1.8}\text{Ca}_{0.2}\text{Mg}_{1.4}\text{Ni}_3$ . The alloys modified by ball milling present better absorption/desorption kinetics than the as-cast alloy. Among the alloys studied, the alloy milled for 20h shows the best overall properties. It can absorb 2.8% hydrogen at 300K and 5wt% hydrogen at 600K within 10 min and desorb 4.98wt% hydrogen at 613K within 10 min.

Three  $\text{Mg}_3\text{RE}$  compounds were prepared in Mg-La, Mg-Nd, Mg-Mm systems, respectively by induction melting in an alumina crucible under protection of pure argon atmosphere [10]. The purity of Mg, La, Nd and Mm is 99.9%. The alloy was melted at about 850°C for 15 min. The estimated loss of Mg by evaporation is 5wt%. The ingots were pulverized by ball milling under argon atmosphere using a Fritch – P5 planetary mill and hydrogenation decrepitation, respectively. The as melted  $\text{Mg}_3\text{La}$ ,  $\text{Mg}_3\text{Mm}$  and  $\text{Mg}_3\text{Nd}$  compounds have good hydrogen absorption kinetic properties even at room temperature.

The alloy with predetermined composition was arc-melted in argon to make button-type ingots weighing about 20g each. To homogenize the alloy composition, the buttons were turned over and remelted five times [11]. They were heat treated in a vacuum furnace. The furnace was evacuated to  $10^{-2}$  torr, heated to 1653K at the rate of 20K/min and held at temperature for 1min. To preserve the high temperature microstructure of the alloy, the buttons were mechanically ground in air to make them into powder form. The substitution of Fe for Cr in the  $\text{Ti}_{0.32}\text{Cr}_{0.43}\text{V}_{0.25}$  alloy was studied. The lattice parameter of the alloy decrease linearly the increasing the Fe ratio. Thus, the logarithmic desorption plateau pressure increased linearly with the decrease of the lattice volume. Heat treatment of Fe containing alloys suppressed the second phase formation a cause for decrease in the effective hydrogen storage capacity but raised the plateau pressure up to several atmospheres. These results suggest a possibility of using ferrovanadium instead of the expensive pure vanadium. However, substituting Fe for Cr had no favorable effect on desorbing residual hydrogen in the BCC phase.

Three  $\text{LaNi}_{4.8}\text{T}_{0.2}$  alloy (with T = Mg, Bi & Sb) were prepared by arc melting of stoichiometric amounts of the pure metals (99.9wt%) in an argon atmosphere. The ingots were homogenized in quartz ampoules under vacuum at 670K for 336hrs. The powder XRD patterns of the alloys were obtained by using STOF powder diffractometer. The hydrides were synthesized and the p – c isotherms were measured using a Sieverts – type apparatus with an operating volume of 5cm<sup>3</sup> adapted for measurements in the range of temperature of 290K – 800K and the pressure of 10MPa. In conclusion, partial substitution of Ni for Al, Mg 7 Bi does not greatly change the hydrogen capacity of these system compared with the original  $\text{LaNi}_5\text{H}_6$ . The substitution of 0.2 Ni atoms in the formula unit by Bi causes an increase in hydrogen content about 13%. This indicates that  $\text{LaNi}_{4.8}\text{Bi}_{0.2}$  hydride can be also considered as a good hydrogen storage material in engineering application [15].

## 2.5 Alloy Fabrication by Ball Milling

All the operations were carried out under pure argon atmosphere [12]. The starting materials were NaH powder (95%, 74  $\mu\text{m}$ , purchased from Sigma-Aldrich Corp.), Al powder (99%, 74 -154  $\mu\text{m}$ ) and Ti powder (99%, 50 - 74  $\mu\text{m}$ ). The Al powder was first ball-milled in the atmosphere of supra-pure  $\text{H}_2$  in order to remove the oxide films on the surface of Al particles. Approximately three grams of sample were prepared each time as follows. The NaH powder and pre-treated Al powder were weighted in 1:1 atomic ratio, and then were mixed with Ti every time in the designated atomic ratio. Three different powders were mixed and introduced into a stainless steel vial together with stainless steel balls. The ball-to-powder weight ratio was 30:1. The vial was then evacuated, filled with 0.5 MPa high purity argon or hydrogen, or 25 ml tetrahydrofuran (THF). The sample was ball-milled for 1-24h at 350 rpm. The composite ball-milled under hydrogen atmosphere has both maximum hydrogen storage capacity and high absorption/desorption rate. The reversible hydrogen storage capacity increases with the increase of Ti content. And the hydriding–dehydriding capacity increase first and then decrease with the prolongation of the milling-time.

Ball milling was done on a Fritsch Planetary Mono Mill pulverisette 6LC-106A with a 250ml stainless steel vessel and stainless steel balls [9]. In these studies, the following parameters were held constant. Milling time (20h), grinding solvent (cyclohexene), carbon precursor (the determinized PSOC1468 coal), solid to solvent ratio (6g: 20ml), ball to sample weight ratio (45:1) and other milling conditions. All the samples were milled at 400rpm in an argon atmosphere to prevent oxidation and minimize air exposure. The research conclude that this reversible hydrogen uptake is a function of temperature but independent of pressure, typical of chemisorptions yet the amount of hydrogen uptake does not correlate to Mg addition and thus appear to be carbon based.

Polycrystalline samples of  $\text{La}_{1-x}\text{Sr}_x\text{Fe}_{1-x}\text{Mn}_x\text{O}_3$  ( $0.3 \leq x \leq 0.7$ ) were prepared by standard solid-state reaction from stoichiometric amounts of  $\text{La}_2\text{O}_3$ ,  $\text{SrCO}_3$ ,  $\text{Fe}_2\text{O}_3$  and  $\text{MnO}_2$ , the purities of which are at least 99.9% [4]. The purity at 99.9%  $\text{La}_2\text{O}_3$  powders was dried for 5h at  $800^\circ\text{C}$  before used. The mixture was ground extensively once again. Then the powder were pressed into pallets and annealed  $1100^\circ\text{C}$  in air for 24h with intermittent grinding and finally cooled the samples down to  $500^\circ\text{C}$  at  $2^\circ\text{C}/\text{min}$  then cooled to room temperature in furnace. The finding for this research, lattice parameter (a) decrease firstly with  $0.3 \leq x \leq 0.5$  and following then increased  $0.3 \leq x \leq 0.7$ . The lattice parameter b and c reduce slightly with coupled substitution of  $\text{Sr}^{2+}$  and  $\text{Mn}^{4+}$  for  $\text{La}^{3+}$  and  $\text{Fe}^{3+}$ .

A powder sample was prepared by deuteration of lanthanum metal (pieces, 99.9% purity) in an autoclave. In a first step the temperature was increased to 673K during 1 day under deuterium gas pressure of about 100 bar. In a second step, the deuterium pressure was released by evacuating the autoclave to  $10^{-2}$  mbar and the temperature was increased to 773K during 1 day. The autoclave was air quenched and opened in an argon filled glove box. The resulting sample was single phase and consisted of cubic  $\text{LaD}_{2+x}$ . The atom relaxations in the  $\text{LaH}_{2+x}$  structure system are of major interest for the study of metal – insulator transitions in this and related systems. Given that the transitions usually occur at slightly sub-stoichiometric compositions they are bound to be affected by such relaxations. The latter could also be related to the

observed decrease in the homogeneity range of the cubic hydride phase of heavy rare-earth elements [5].

Alloy has been prepared by ball milling process in benzene atmosphere. This process believes that benzene has relatively faster absorption desorption kinetics. The characterization process conditions that have been set to the pressure between 10 to 140 psi and the temperature between 308K – 338K. The outcome of this experiment is that the ideal operating condition for  $\text{La}_{0.23}\text{Ni}_{0.34}\text{Nd}_{0.008}\text{Ti}_{0.01}\text{Al}_{0.01}$  and thermodynamics of formation of hydride are pressure between 10 to 140 psi and the temperature between 308K – 338K [13].

## 2.6 Mechanical Alloying

$\text{LaMg}_2\text{Ni}$  coarse crystals have been obtained by slowly cooling the liquid alloy in a BN crucible to reduce magnesium evaporation in an induction furnace. Nanostructure powders have been obtained by mechanically grinding the as – cast alloy.  $\text{LaMg}_2\text{Ni}$  has also been obtained by mechanically alloying the parent elements for 110hrs. Mechanical treatments were carried out in commercial mixer – mill. The structure was analyzed by XRPD. After the experiment, there are four conclusions that can be made. First, nanostructured  $\text{LaMg}_2\text{Ni}$  can be obtained by mechanical alloying. Second, hydrogenation of the samples under a pressure of hydrogen of 0.4MPa at room temperature leads the formation of a La – hydride phase with contribution of an amorphous phase. Lastly, absorption under reactive milling enhanced very much the absorption rate. Lastly, thermal desorption up to 983K of hydrogenated alloys leads again to parent  $\text{LaMg}_2\text{Ni}$  phase [14].

## 2.7 Scanning Electron Microcopy (SEM)

The microstructure of  $\text{MgH}_2$  catalyzed with nano-particle and  $\text{Nb}_2\text{O}_5$  were investigated by SEM & TEM observations. Hydrogen desorption properties of both composites after the ball-milling have been examined and they showed almost same

properties, where the amount of ~6mass% hydrogen is desorbed in the temperature range from 150°C to 250°C at heating rate 5°C/min under He flow. The different distribution states of additive between two compounds are characterized as follows. The MgH<sub>2</sub>-Ni nano composite, the metal Ni nano particles are found in the BSE image. Ni particles with smaller diameters than 1µm are uniformly distributed on the MgH<sub>2</sub> particles with smaller diameters than 5µm. (Hanada et al.)

Microstructure analysis showed that unimodal size distribution, characteristic for the starting material size distribution for the sintered samples. The grain diameters range was divided into three sub ranges in the cases of materials sintered at 1200°C and 1300°C and into two subintervals for the material sintered at 1380°C. As the sintering temperature rises up to 1300°C and 1380°C enhanced surface reactivity leads to the intensification of the transport processes resulting less porous and denser microstructure. As result of the mass transport between the grains which occur at these temperatures, we have noticed that the grains with a smaller number of boundaries grow, while grains with a smaller number of boundaries decrease. (Pavlovic et al)

## 2.8 (Thermo Gravimetric Analysis)TGA

TGA curves for the powders. As a conservative estimate the quantity of desorbed hydrogen was always calculated from the weight loss between the tangent lines A, B and C at the temperature range corresponding to highest rate of weight loss (hydrogen desorption). Furthermore, the Mg with V and Y composite powders exhibit a two-step desorption. To explain this two-step desorption. To explain this two-step powder desorption phenomenon Mg + 10wt.%V and Y composite powders were desorbed in TGA apparatus at 350°C. Apparently, in these two composites with V and Y, a partial desorption of hydrogen from β-MgH<sub>2</sub> occurs in TGA at temperatures up to 350°C. (Czujko et al.)



## 2.9 Fourier Transform Infra Red (FTIR)

According to the literature, these bands are characteristic of terminally bonded M-H stretching absorptions in the region  $1900 \pm 300 \text{ cm}^{-1}$  and of hydrogen in a position bridging two or more metals and in which the hydrogen mode is shifted to lower energy,  $1100 \pm 300 \text{ cm}^{-1}$ . Certain lanthanides and actinides, such as La and U are known to react with hydrogen and yield metal hydrides. According to this report, a series of non-stoichiometric hydrides are formed between  $\text{LaH}_2$  ( $\text{CaF}_2$ ) structure and  $\text{LaH}_3$  bands at  $540$  and  $1000 \text{ cm}^{-1}$  is attribute to  $\text{LaH}_2$  and it is shifted to lower energies with increasing hydrogen concentration. (Bettelheim et al.)

## 2.10 Summary

Table 1 Summary of methods and materials of previous researcher.

Researcher	Material	Method	Findings
Shih et al.(2006)	$\text{LaNi}_{4.25}\text{Co}_{0.5}\text{V}_{0.1}$	-Arc melting, <ul style="list-style-type: none"> <li>○ -Annealing at <math>1100^\circ\text{C}</math> under vacuum for 10h</li> <li>○ -Pressed at pressure of <math>125 \text{ kg/cm}^2</math> to form pallet.</li> <li>○ - Sintered in vacuum at <math>450</math> or <math>700^\circ\text{C}</math> for 5h</li> </ul>	Hydrogenation are approximately 8% and 5%
Wang et al.(2006)	$\text{LaNi}_{4.25}\text{Al}_{0.75}$	Vacuum melting of La and Ni component with subsequent addition of aluminium	Good material for hydrogen isotopes storage.

		to the melt, and the composition was determined by method of chemical analysis	
Gao et al.(2005)	$\text{La}_{1.8}\text{Ca}_{0.2}\text{Mg}_{14}\text{Ni}_3$	<ul style="list-style-type: none"> <li>- Ball milling. <ul style="list-style-type: none"> <li>○ Milling time (20h)</li> <li>○ Ball: powder = 20:1</li> <li>○ Liquid : solid = 6: 1</li> <li>○ Speed = 350 rpm</li> </ul> </li> </ul>	<ul style="list-style-type: none"> <li>- Hydrogenation at 300K = 4.1%</li> <li>- Hydrogenation at 600K = 5.1 %</li> </ul>
Chio et al. (2007)	$\text{LaMg}_2\text{Ni}$	<ul style="list-style-type: none"> <li>- Mechanical alloying <ul style="list-style-type: none"> <li>○ Time: 110hrs</li> </ul> </li> </ul>	<ul style="list-style-type: none"> <li>- Hydrogenation under a P= 0.4MPa at room temperature leads the formation of a La – hydride phase.</li> <li>- Thermal desorption up to 983K.</li> </ul>
Jain et al. (2007)	$\text{La}_{0.23}\text{Ni}_{0.34}\text{Nd}_{0.008}\text{Ti}_{0.01}\text{Al}_{0.01}$	<ul style="list-style-type: none"> <li>- Ball milling <ul style="list-style-type: none"> <li>○ Benzene atmosphere</li> </ul> </li> </ul>	<ul style="list-style-type: none"> <li>Ideal condition for alloy to operate : P = 10 – 140 psi T = 308K – 338K</li> </ul>
Giza et al. (2006)	$\text{LaNi}_{4.8}\text{T}_{0.2}$ alloy (with T = Mg, Bi & Sb)	<ul style="list-style-type: none"> <li>- Arc melting in argon atmosphere.</li> </ul>	<ul style="list-style-type: none"> <li>The substitution of 0.2 Ni atoms in the formula unit by Bi causes an increase in hydrogen</li> </ul>

			content about 13%.
Hanada et al. (2006)	SEM and TEM characterization of magnesium hydride catalyzed with Ni nanoparticle or Nb <sub>2</sub> O <sub>5</sub>	- Mechanical alloying - Ball milling	Adsorp hydrogen 4.5 mass % in the pressure of 1 MPa within 15s.

## CHAPTER 3

### MATERIALS AND METHODS

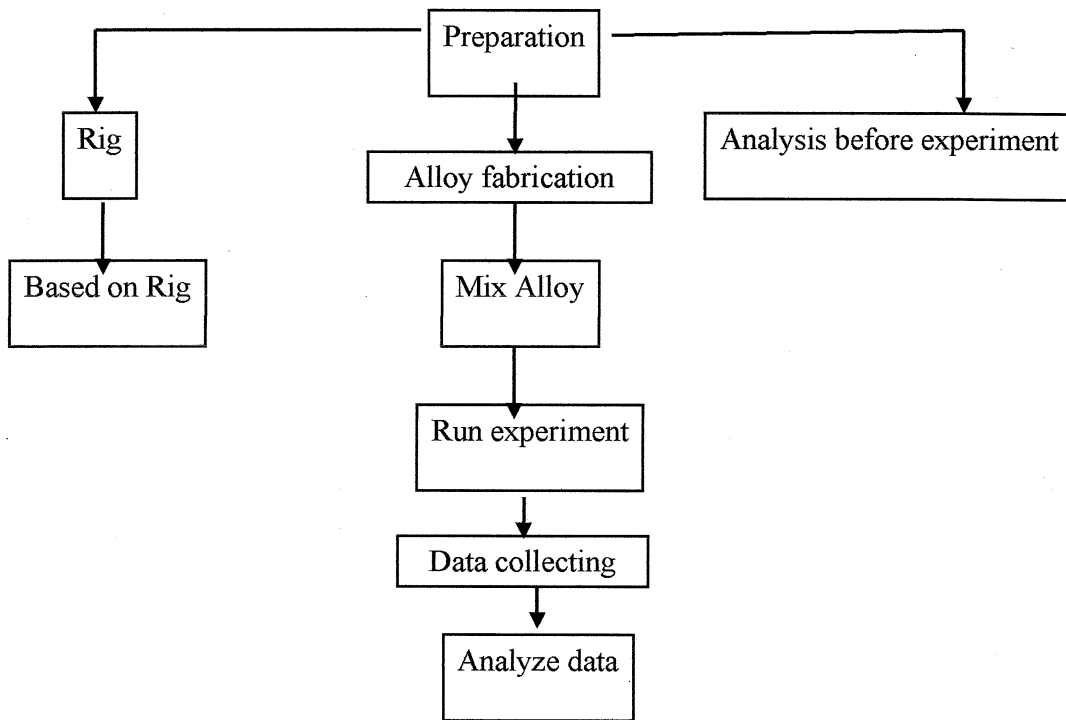


Figure 2 Methodology

### 3.1 Materials & Apparatus

- I. Lanthanum oxide ( $\text{La}_2\text{O}_3$ )
- II. Iron oxide ( $\text{Fe}_2\text{O}_3$ )
- III. Manganese oxide ( $\text{MnO}_2$ )
- IV. Tetrahydrofuran (THF)
- V. Gas tubing  $\frac{3}{4}$  inch
- VI. Ball valve  $\frac{1}{2}$  inch
- VII. Connector  $\frac{1}{2}$  inch
- VIII. Steel pipe ( $d = 4$  inch)
- IX. Hydrogen gas (99.9% purity)

### 3.2 Equipment

- I. Furnace
- II. Scanning electron microscopy (SEM)
- III. Thermal gravimetric analysis (TGA)
- IV. Fourier Transform Infra Red (FTIR)
- V. Heating plate
- VI. Water Bath
- VII. Hydrogen Regulator

### 3.3 Preparation

#### 3.3.1 La based alloy

- I. Selection of material
- II. Sample is choose which is  $\text{LaFeMn}$  with the formula of  $\text{La}_{1-x}\text{Fe}_x\text{Mn}$  ( $0 < X < 1$ ) ( $X = 0.05, 0.1, 0.2$ )
- III. The alloy based on 10g of mass per alloy
- IV. Using molecular weight of alloy to determine the total mole of alloy

- V. Calculation is shown in appendices 1.
- VI. Weight the metal element according to calculations that have made
- VII. The 3 elements were mixed in the stirrer with addition of THF liquid for 4 hrs.
- VIII. Then, the mixtures are prepared using sintering process by inserting it into the furnace in the temperature of 500°C for 5 hrs.

### 3.3.2 Rig

- I. Based on the drawing.(details on rig refer figure 3)

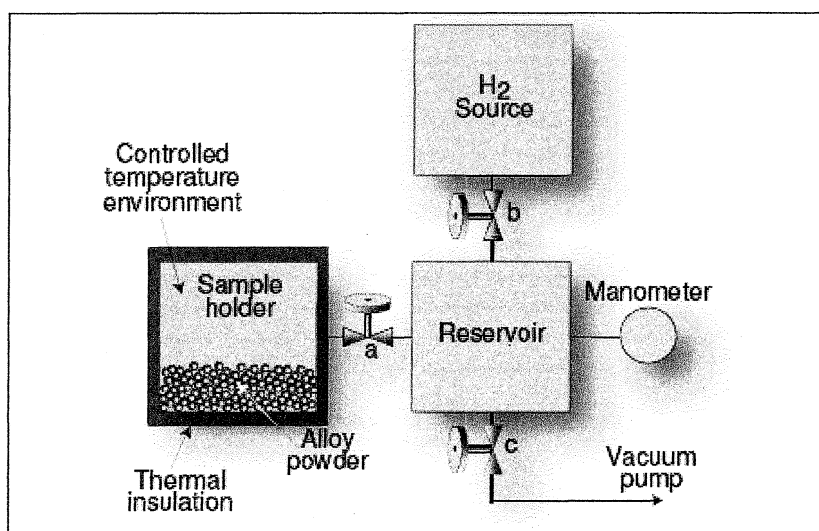


Figure 3 Test rig for the experiment

### 3.4 Analysis before experiment

- I. Use SEM for microstructure analysis of the alloy after the sintering process. All the procedure to operate the SEM is done by the staff in charge. The magnifier size of the microstructure is set to 1000. the grain size to be set is 10 $\mu$ m.
- II. The TGA was used to determine the thermal stability of the alloy oxide. The TGA ramping temperature was set at 10°C/min and the temperature that has been set is 500°C. The TGA curve was analyze after the analysis was done.

### 3.5 Running the experiment

#### 3.5.1 General procedure for rig operation: (based on figure 2)

- I. The range of pressure that conducting in this rig is between 0.5 bar – 3 bar.
- II. The range of operating temperature in this rig is between 20°C - 100°C.
- III. Valves **a** and **c** are open and valve **b** is closed.
- IV. The sample is degassed by heating it to a high temperature and extracting the released vapors by means of a vacuum pump.
- V. Valves **a** and **c** are then closed and **b** is opened
- VI. A known volume of hydrogen at known pressure and temperature, i.e., with a known amount of the gas.
- VII. With **b** and **c** closed, **a** is opened and hydrogen is absorbed.
- VIII. This causes the temperature of the powder to rise because the absorption is exothermic.
- IX. The system is then allowed to return to the initially selected temperature and the equilibrium pressure is observed

#### 3.5.2 Details procedure of hydrogenation process (refer figure 3)

##### a. Safety & leakage testing

- I. Test the maximum pressure that rig can operate.
- II. Used bubble soap to detect the leakage between joining.
- III. If any leakage detected, reassemble back the joining.
- IV. Purge the air inside the tubing using inert gas such as nitrogen (N<sub>2</sub>)
- V. Flow the hydrogen gas for a while to detect any leakage using gas analyzer.

b. Operating procedure for alloy activation process

- I. Placed the alloy in the reactor.
- II. Closed the reactor lid tightly.
- III. Set the outlet pressure 0.5 bar at the regulator.
- IV. Open V1 to ensure the hydrogen flow into the reservoir. V2, V3, V4 & V5 are closed.
- V. After the pressure in the reservoir achieve 0.5 bar closed the gas supply.
- VI. Open the V3 & V4 to flow the gas into the reactor.
- VII. When the pressure is not achieved 0.5 bar in the reactor supply more gas slowly until 0.5 bar is achieved.
- VIII. Let the sample activated for 1 day.

c. Hydrogenation process

- I. Set pressure outlet at 1bar.
- II. Set the temperature at 80°C at the water bath.
- III. Put the alloy in the reactor and closed the lid tightly
- IV. Open V1 to ensure hydrogen flow into the reservoir. V2, V3, V4 & V5 are closed.
- V. After the pressure in the reservoir achieve 1 bar closed the gas supply.
- VI. Open the V3 & V4 to flow the gas into the reactor.
- VII. If the pressure not achieved 1 bar in reactor supply more gas slowly until 1 bar is achieved.
- VIII. Closed V3 & V4.
- IX. Start the timer to determine the interval for hydrogenation process.
- X. Monitor the pressure gauge to detect any pressure drop
- XI. Once the pressure drop happen, it means hydrogenation process is occur and at the same time write down the time taken to start the hydrogenation process.



- XII. Refer 3.6.1 to measure the adsorption performance of the alloy
- XIII. After done doing step 3.6.1 continue the experiment based on the interval time that obtained.
- XIV. Run the experiment until the data that obtained were at constant value.
- XV. Repeat the experiment for pressure at 1 bar at temperature 90°C, pressure at 2 bar and temperature at 80°C and at pressure 2 bar at temperature at 90°C.

### 3.6 Data Collecting

#### 3.6.1 Alloy mixing

- I. Record the physical changes during the mixing process.
- II. The time taken for the mixing process to occur.

#### 3.6.2 Adsorption performance

- I. Weight the mass of reactor before the experiment
- II. Weight the 2.5g of alloy.
- III. Weight the mass of reactor after the experiment
- IV. Determine the mass of hydrogen has been adsorbing using this formula. Mass of hydrogen = total reactor mass after experiment - mass of reactor – mass of metal hydride
- V. Calculate hydrogen mass percentage.

#### 3.6.3 Fourier Transform Infra Red (FTIR)

- I. Follow the instruction manual given by the person in charge.
- II. The sample peak was observed and the wavenumbers was selected and showed at the bottom of the peak.
- III. The spectrum of the 3 samples was analyzed to determined whether hydriding process occur or not.

### 3.7 Analyzing data

#### 3.7.1 Microstructure of alloy

- I. Compare the pore size of the 3 samples that analyzed.

#### 3.7.2 TGA analysis

- I. Calculate the weight loss of the 3 samples.
- II. The method that have been used id tangent method and summarized in Table 3.

#### 3.7.3 FTIR analysis

- I. The spectrum are observe and determine the compound that exist after the hydrogenation process.

#### 3.7.2 Adsorption performance

- I. The weight loss or gain is calculated and the percentage is determined.
- II. The processes that occur are determined based on the weight differential.

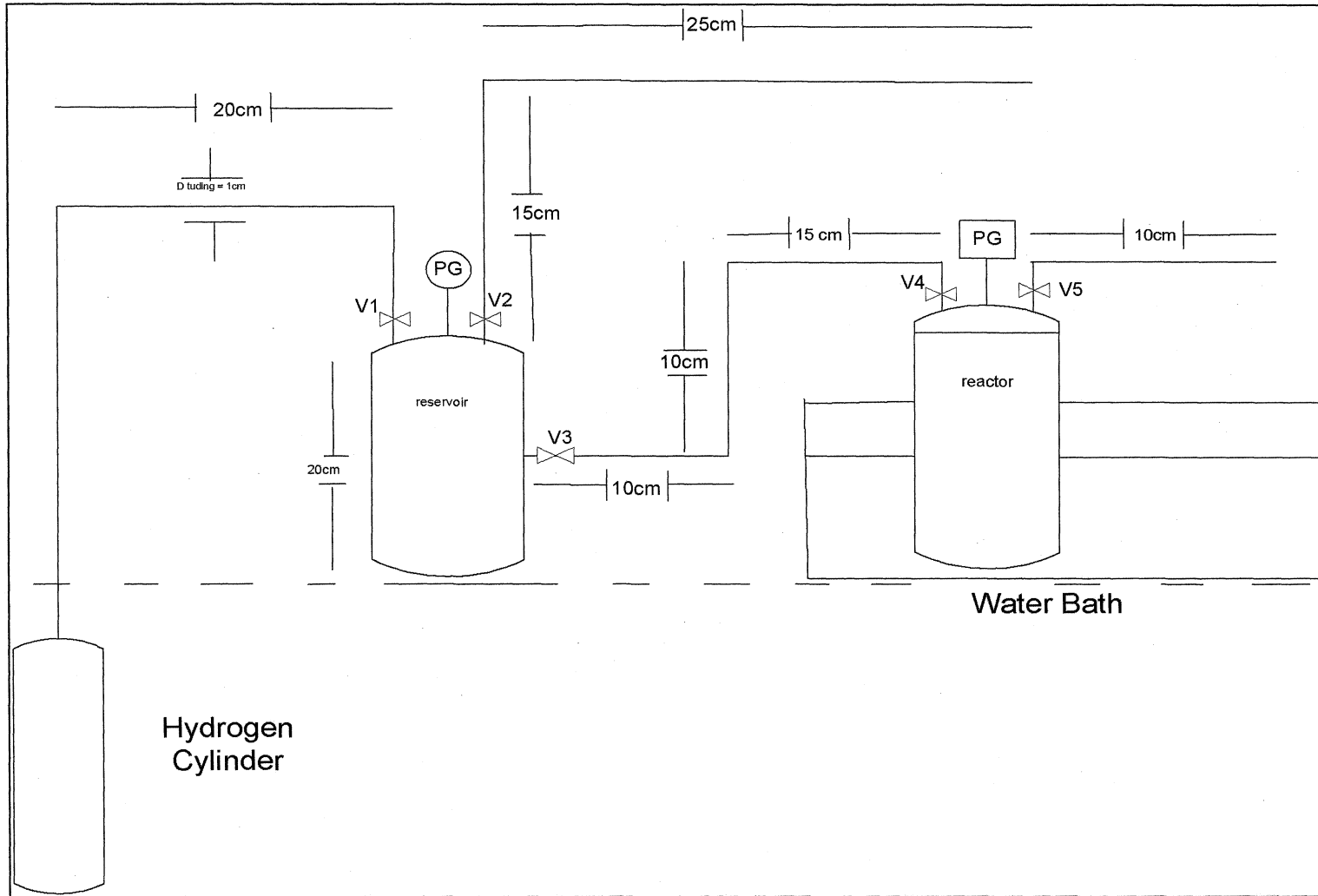


Figure 4 Test Rig for Hydrogenation Process

## CHAPTER 4

### RESULTS & DISCUSSION

#### 4.1 Alloy Fabrication

Table 2 Observation During the Mixing Process

La <sub>1-x</sub> Fe <sub>x</sub> Mn	Observation	
	Before mixing	After mixing
X = 0.05	<p><u>Physical characteristic (color)</u>            La<sub>2</sub>O<sub>3</sub> = white powder            Fe<sub>2</sub>O<sub>3</sub> = Black powder            MnO<sub>2</sub> = Black powder</p> <p><u>After adding with THF</u>            The mixing has two layers which is liquid and solid at the bottom.</p>	<p><u>Physical characteristic (color)</u>            The mixture becomes grey in color due of the high amount of La<sub>2</sub>O<sub>3</sub> in the mixture. The time for mixing process is only 2hrs in the fume hood. The mixture splash a lot when the mixture nearly dry when heating using heating plate.</p>
X = 0.1	<p><u>Physical characteristic (color)</u>            La<sub>2</sub>O<sub>3</sub> = white powder            Fe<sub>2</sub>O<sub>3</sub> = Black powder            MnO<sub>2</sub> = Black powder</p> <p><u>After adding with THF</u>            The mixing has two layers which is liquid and solid at the bottom.</p>	<p><u>Physical characteristic (color)</u>            The mixture becomes black in color due of the high amount of Fe<sub>2</sub>O<sub>3</sub> &amp; MnO<sub>2</sub> in the mixture. The time for mixing process is only 2hrs in the fume hood. The mixture splash a little when the mixture nearly dry when heating using heating plate.</p>
X = 0.2	<p><u>Physical characteristic (color)</u>            La<sub>2</sub>O<sub>3</sub> = white powder            Fe<sub>2</sub>O<sub>3</sub> = Black powder            MnO<sub>2</sub> = Black powder</p> <p><u>After adding with THF</u>            The mixing has two layers which is liquid and solid at the bottom.</p>	<p><u>Physical characteristic (color)</u>            The mixture becomes blacker in color due of the high amount of Fe<sub>2</sub>O<sub>3</sub> &amp; MnO<sub>2</sub> in the mixture. The time for mixing process is only 2hrs in the fume hood. The mixture splash a little when the mixture nearly dry when heating using heating plate.</p>

## 4.2 Characterizations

### 4.2.1 Microstructure analysis (SEM)

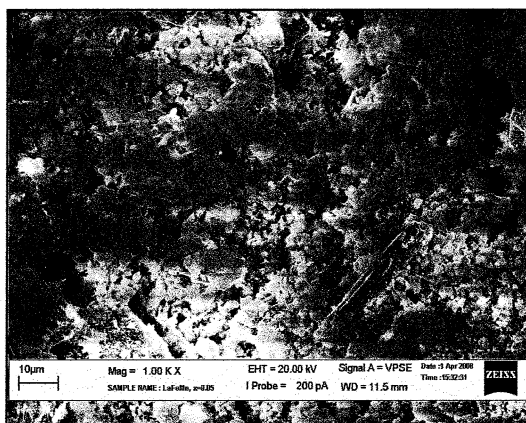


Figure 5 SEM image of  $(La_{1-x}Fe_xMn)$  oxide,  $x=0.05$

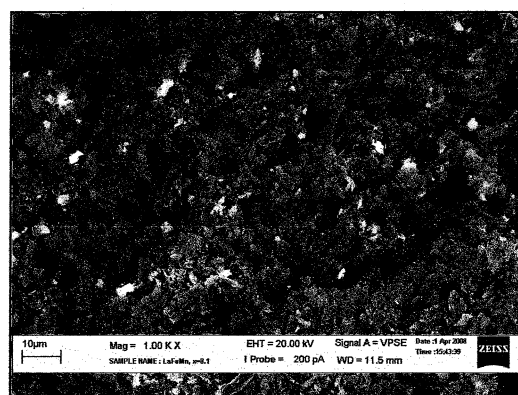


Figure 6 SEM image of  $(La_{1-x}Fe_xMn)$  oxide,  $x=0.1$

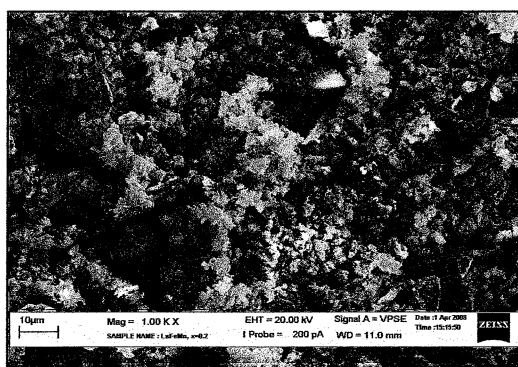
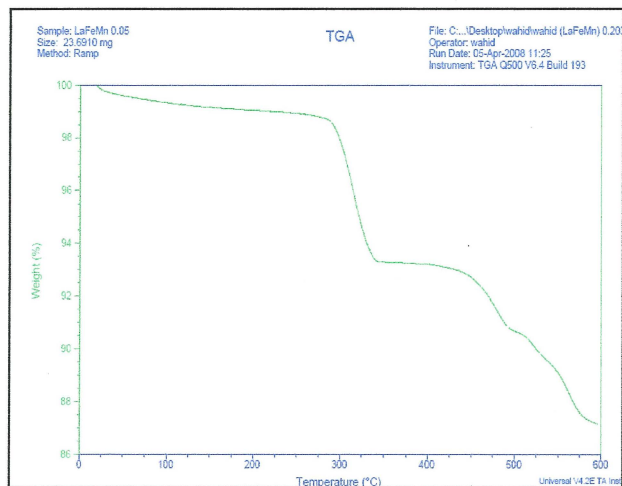
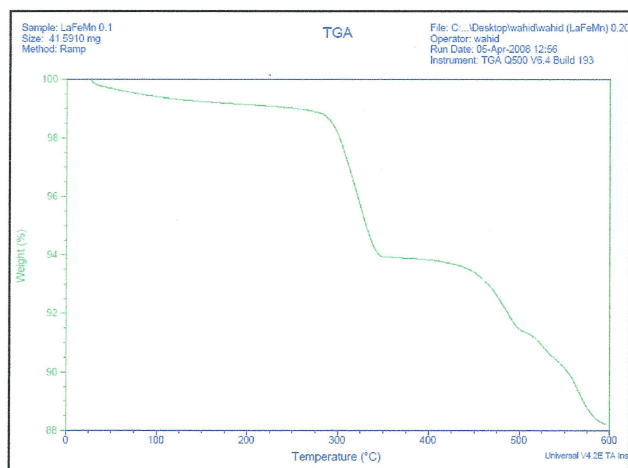


Figure 7 SEM image of  $(La_{1-x}Fe_xMn)$  oxide,  $x=0.2$

Based on the BSE image, Figure 5 that produced by the SEM, we can see that the microstructure of  $\text{La}_{1-x}\text{Fe}_x\text{Mn}$ ,  $x = 0.05$ . The image was magnified to 1000 times and the size of the grain that focused is  $10\mu\text{m}$ . The white particles that scattered mostly in the image are the lanthanum oxide powder which is white in color. This is happen due to the highest mole fraction of lanthanum oxide in the alloy. From this image we can see that the pore size within this alloy which rich of lanthanum oxide have the smallest pore. Figure 6 is the image produced by the SEM, we can see that the microstructure of  $\text{La}_{1-x}\text{Fe}_x\text{Mn}$ ,  $x = 0.1$ . The image was magnified to 1000 times and the size of the grain that focused is  $10\mu\text{m}$ . The white particles that scattered in the image are the lanthanum oxide powder which is white in color and the black particles are manganese oxide and iron oxide. This is happen due to the less mole fraction of lanthanum oxide in the alloy. From this image we can see that the pore size within this alloy which rich of manganese oxide and iron oxide is medium. Based on Figure 7 that produced by the SEM, we can see that the microstructure of  $\text{La}_{1-x}\text{Fe}_x\text{Mn}$ ,  $x = 0.2$ . The image was magnified to 1000 times and the size of the grain that focused is  $10\mu\text{m}$ . The white particles that scattered in the image are the lanthanum oxide powder which is white in color and the black particles are manganese oxide and iron oxide. This is happen due to the less mole fraction of lanthanum oxide in the alloy. From this image we can see that the pore size within this alloy which rich of manganese oxide and iron oxide is big. From the SEM image that obtained, we can see that the pore size of the alloy is important to ensure the hydrogen adsorption is occur because the bigger the pore size the higher adsorption rate that will produce by the alloy. The alloy that have been fabricated id not produced big pore size due to the process that was chosen was sintering which is reduce the pore size because when sintering process occur the particles that contain high grain number intent to expend their boundaries. From the figure 5, 6 and 7 we can see that Figure 7 have the biggest pore that can adsorb hydrogen in higher percentage but unfortunately the reduction process occur because of the oxide that exist in the alloy (Czujko et al.). In the result of performance show that the  $x = 0.2$  show the low value of reduction which mean it intend to do adsorption which can conclude that the bigger pore size the less reduction process.

## 4.2.2 Thermal Gravimetric Analysis (TGA)

Figure 8 TGA curve of  $(La_{1-x}Fe_xMn)$  oxide,  $x=0.05$ Figure 9 TGA curve of  $(La_{1-x}Fe_xMn)$  oxide,  $x=0.1$

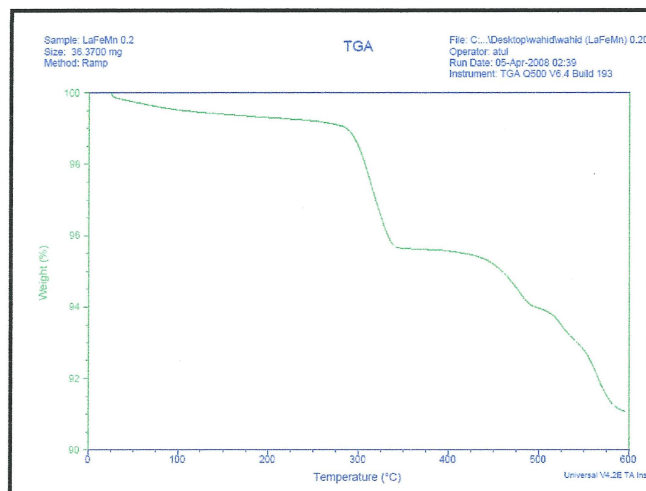


Figure 10 TGA curve of  $(La_{1-x}Fe_xMn)$  oxide,  $x=0.2$

Table 3 Weight loss percentage / temperature

$La_{1-x}Fe_xMn$	Weight loss(%) / Temperature(°C)			Metal oxide reduction(wt%)/ $\Delta T$ °C
	Tangent line A	Tangent line B		
	a	b	c	
X= 0.05	0.0400	0.0225	0.0150	0.175
X = 0.1	0.03	0.0267	0.0333	0.04
X= 0.2	0.0150	0.0167	0.0100	0.025

Based on the figure 8, 9 And 10 the TGA graph show us the percentage of weight loss versus time in the environment of rich  $N_2$  in the temperature of 600°C. The ramping temperature for this process is 10°C /min. As a conservative estimation the quantity of oxygen reduction was always calculated from weight loss between tangents lines A & B at the temperature range corresponding to the highest rate of weight loss (oxygen reduction). Table 2 shows the reduction onset and end temperatures, corresponding weight loss and amount of oxygen released. From table 2 we can see that  $x = 0.05$  have the highest reduction rate compare to  $x = 0.1$  and  $x= 0.2$ . This is happening due to the lanthanum oxide fraction that was very big in the  $La_{1-x}Fe_xMn$  that caused the reduction process because of the unstable or decomposition of  $La_2O_3$  during heating process.



## 4.2.3 FTIR

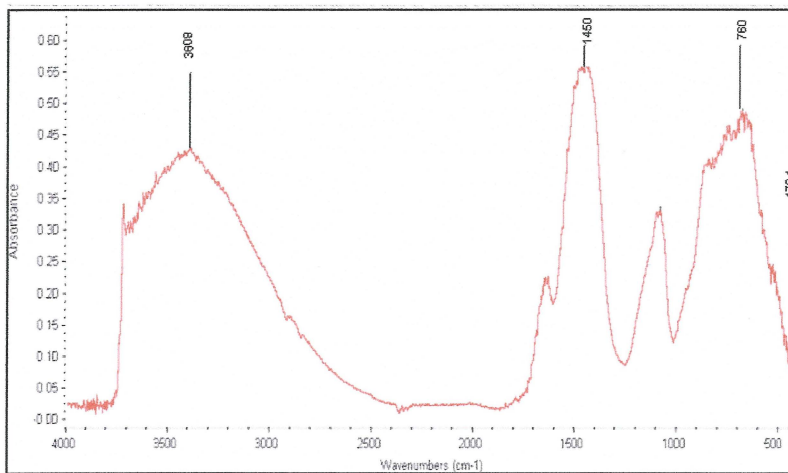
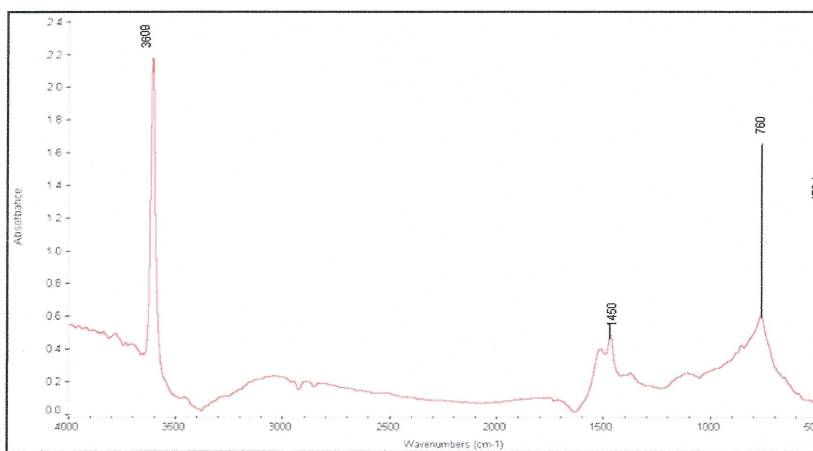
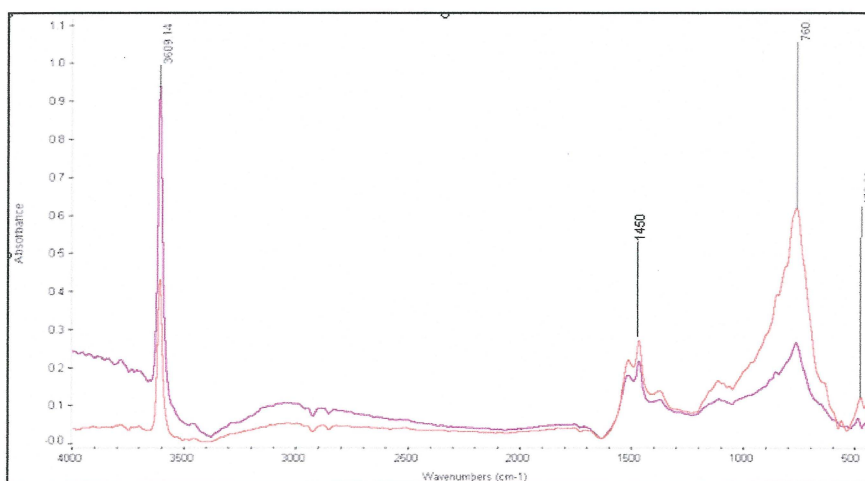
Figure 11 Spectrum of  $(La_{1-x}Fe_xMn)$  oxide,  $x=0.05$  after hydriding processFigure 12 Spectrum of  $(La_{1-x}Fe_xMn)$  oxide,  $x=0.1$  after hydriding processFigure 13 Spectrum of  $(La_{1-x}Fe_xMn)$  oxide,  $x=0.2$  after hydriding process

Table 4 Position of FTIR bands of lanthanum hydrides according to the present work and the literature

Hydride ( $2 \leq n \leq 3$ )	Band position/cm-1 according to:		
	Present work		literature
	Electrochemical hydrogenation	Hydrogen adsorption	
LaH <sub>n</sub>	472 831 1021 1401,1696 566,685,738 856,910	566,793 856,1017	540 <sup>b</sup> 750-850 <sup>b</sup> 1000 <sup>b</sup>  970 ± 60 <sup>c</sup>

a - only spectrochemical experiments were performed

b - Based on FTIR measurements of Ref A. Fujimori, M. Ishii, and N. Tsuda, Physical Status Solidi B, (1980)

c - Based on inelastic neutron scattering measurements of J.J Rush, H.E Flotow, D.W. Connor and C.L, Thaper, J. Chemical Physical (1966)

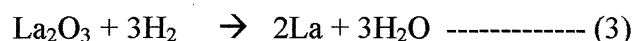
The bands observed appear at 3609, 1450, 760 and 473.61 cm<sup>-1</sup>. According to Ashley et al. these characteristic of terminally bonded M-H stretching absorptions in the region 1900 ± 300 cm<sup>-1</sup> and hydrogen in a position bridging two or more metals and which the hydrogen mode is shifted to lower energy, 1100 ± 300 cm<sup>-1</sup>. Certain lanthanide such as lanthanum to react with hydrogen and to yield metal hydrides. It can be seen from table 3 that 4 bands are observed in the 400 – 3609 cm<sup>-1</sup> region for lanthanum hydrides in the present work (472, 831, 1021 cm<sup>-1</sup>). These results are in agreement with those reported in the literature (Fujimori et al) for lanthanum hydrides obtained by the adsorption of hydrogen in lanthanum melt. According to this report, a series of non stoichiometric hydrides are formed between LaH<sub>2</sub> (CaF<sub>2</sub> structure) and LaH<sub>3</sub> bands at 540 and 1000 cm<sup>-1</sup> are associated with LaH<sub>3</sub> at the band 850 cm<sup>-1</sup> is attribute to LaH<sub>2</sub> and shifted to lower energies with increasing hydrogen concentrations. Based on the spectrum that obtained after hydriding and the with the comparison with the previous journal the peak that are possibly lanthanum hydride are 760 cm<sup>-1</sup> based on the table 3 value which is the range of 750-850<sup>b</sup> cm<sup>-1</sup>. Based on the journal Serbia et al. the value for iron oxide is 476 cm<sup>-1</sup> within the range of 460 ± 30 cm<sup>-1</sup>.

### 4.3 Reduction percentage

Table 5 Percentage of reduction ( $\text{La}_{1-x}\text{Fe}_x\text{Mn}$ ) oxide in operating condition at  $P= 2\text{bar}$ ,  $T= 100^\circ\text{C}$  and  $t = 1\text{ hr}$ .

x	Initial weight(g)	Final weight(g)	Weight loss(g)	Weight loss (%)
0.05	23.5	23.4760	0.0240	0.102
0.1	23.5	23.4800	0.0200	0.085
0.2	23.5	23.4813	0.0187	0.080

Based on the table 5, the percentage of weight loss is calculated to determine which composition have high rate of reduction.  $X= 0.05$  intend to occur reduction process rather than hydrogenation process. This is happening due to the pore size of  $x =0.05$  that is very small and the hydrogen could not adsorp in the alloy. Due to the unstable of  $\text{La}_2\text{O}_3$  which is approve by TGA curve that show us  $x= 0.05$  have the highest weight loss which can related to this table 4 that show us the weight loss of  $x =0.05$  is 0.102%. The  $x = 0.2$  contribute the lowest weight lost which is 0.08% and this is happening due to the big pore size that might interact hydrogen to adsorp to the metal even the reduction process occur but there are hydrogenation happen that prove by FTIR result which is the identification of  $\text{LaH}_n$  with the band of  $760\text{cm}^{-1}$  peak which compare to the previous research. The possible Reduction equation that occurs during reduction process in this study is:



## CHAPTER 5

### CONCLUSION & RECOMENDATION

In conclusion the high value of the mol fraction of base (x) the high value of weight loss that occur. The  $x = 0.05$  have the highest weight loss which is 0.102 %. The high percentage of lanthanum base inside the alloy decreases the pore size of the alloy that contribute the factor of hydrogenation process. The unstable of lanthanum oxide also contribute due the oxygen reduction when hydrogen was flow into the alloy. Even though the reduction occur in this experiment but there is still hydrogenation process occur that prove by the FTIR result which the wavelength of  $\text{LaH}_n$  was detected using the range value of previous research. The value which shows the occurrence of  $\text{LaH}_n$  is at the band  $760\text{cm}^{-1}$ . This experiment proves that the influence of temperature and pressure produce the higher adsorption or reduction rate.

In my recommendation I would like to recommend that in further research:

- I. Used pure metals rather than oxide metals because oxygen intends to produce reduction process which causes weight loss to the alloy.
- II. The method of alloy preparation also important because when we use sintering process the high number grain will expend their boundaries and cause the decrease of pore size that make the alloy hard to adsorp hydrogen. Ball milling is the best method to increase the percentage of hydrogenation process because the ball milling increase the surface area that contact to the hydrogen and increase the pore size of the alloy.
- III. The temperature also plays an important role in hydrogen adsorption. The temperature that we used is only  $100^\circ\text{C}$  which not enough to increase the kinetic of the alloy. In my recommendation also I want to recommend

using heating jacket to increase the temperature into 500°C. The pressure also needs to be high to force the hydrogen adsorp into the alloy but operating in high pressure is risky and need to be concern of the safety of the person operate the rig and the maximum pressure design for the rig.

## REFERENCES

- Bent Sorensen (2004). Hydrogen and Fuel Cells Emerging technologies and applications. (2<sup>nd</sup> ed.)
- M. Stange, J.P Maehlan, Yartys, P. Norby, W. van Beek, H. Emerich (2005). In situ SR-XRD studies of hydrogen absorption-desorption in  $\text{LaNi}_{4.7}\text{Sn}_{0.3}$ . J. of Alloys Comp. 404-406 (2005) 604-608.
- RJ Shih, Y. Oliver, T-P. Perng. (2006). Self-supported electrodes made of  $\text{LaNi}_{4.25}\text{Al}_{0.15}\text{Co}_{0.5}\text{V}_{0.1}$  and Ag or Ni for hydrogenation. International J. of Hydrogen Energy 31 (2006) 1716-1720
- G.Y Huo, Y. Qing, F. Dong, D. Song, (2006). Preparation and characterization of series  $\text{La}_{1-x}\text{Sr}_x\text{F}_{1-x}\text{Mn}_x\text{O}_3$  ( $0.3 \leq x \leq 0.7$ ) compounds (B2002102)
- G. Renaudin, k. Yvon, W. Wolf, P. Herzig. (2005). Atom Relaxation around hydrogen defects in lanthanum hydride. J. of Alloys Comp. 404-406(2005) 55-59
- H.H. Cheng, H.G. Yang, S.L. Li, X. X Deng, D.M Chen, K. Yang (2006) Effect of Hydrogen absorption/desorption cycling on hydrogen storage performance of  $\text{LaNi}_{4.25}\text{Al}_{0.75}$ . J. of Alloys and Compounds.
- W. Wang, X.G. Long, G.J. Cheng, S. M. Peng, B. F. Yang (2006) Tritium absorption – desorption characteristics of  $\text{LaNi}_{4.25}\text{Al}_{0.75}$ . J. of Alloys Compounds.
- L.H Gao, C.P. Chen, L.X. Chen, X. Wang, J. Zhang, X. Xiao, Q. Wang, (2005)

Hydriding /dehydriding behaviors of La<sub>1.8</sub>Ca<sub>0.2</sub>Mg<sub>14</sub>Ni<sub>3</sub> alloy modified by mechanical ball-milling under argon. J. of Alloys Compounds.

Deepa L. Narayanan and Angela D. Lueking (2006)

Mechanically milled coal and magnesium composites for hydrogen storage.  
Volume 45, Issue 4, April 2007, Pages 805-820.

L.Z. Ouyang, H.W. Dong, C.H. Peng, L. Xian and M. Zhu, (2002)

A new type of Mg-based metal hydride with promising hydrogen storage properties. International J. of Hydrogen Energy.

Jeong-Hyun Yoo, Gunchoo Shim, Sung-Wook Cho and Choong-Nyeon Park,(2005)

Effects of desorption temperature and substitution of Fe for Cr on the hydrogens storage properties of Ti<sub>0.32</sub>Cr<sub>0.43</sub>V<sub>0.25</sub> alloy. International J. of Hydrogen Energy.

Xuezhang Xiao, Lixin Chen, Xinhua Wang, Qidong Wang and Changpin Chen(2004)

The hydrogen storage properties and microstructure of Ti-doped sodium aluminum hydride prepared by ball-milling International J. of Hydrogen Energy.

Ankur Jain,R.K. jain, Shivani Agarwal, I.P. Jain. (2007)

Structural and thermodynamical investigations of La<sub>0.23</sub>Ni<sub>0.34</sub>Nd<sub>0.008</sub>Ti<sub>0.01</sub>Al<sub>0.01</sub> hydrogen storage alloy. International J. of Hydrogen Energy.

M. Di Chio, L. Schiffrini, S. Enzo, G. Cocco, M. Baricco. (2007)

Hydride phase formation in LaMg<sub>2</sub>Ni during H<sub>2</sub> formation. Renewable Energy 33(2008) 237 240.

K. Giza, W. iwasieczko, V.V. pavlyuk, H. Bala, H. Drulis. (2007)

Thermodynamical properties of La – Ni – T (T= Mg, Bi and Sb) hydrogen storage systems.

O. Ostrovski, G. Zhang, D.S. Liu, R. Kononov, A. Adipuri, S.A. Rezan, and A.R. Muhammad (2006) Reduction of Stable Metal Oxides

N.N. Greenwood and A. Earnshaw (2005)Chemistry of the Elements (6<sup>th</sup> ed.)

N. Hanada, E. Hirotooshi, T. Ichikawa, E. Akiba, H. Fujii (2006)

SEM & TEM characterization of magnesium hydride catalyzed with nanoparticle Nb<sub>2</sub>O<sub>5</sub>

- V. Pavlovic, D. Petrovic, Z. Nikolic, V. Pavlovic (2006)  
Automatic Microstructure analysis of Sintered Materials.
- T. Czujko, R.A Varin, C. Chiu, Z. Wronski. (2005)  
Investigation of the hydrogen desorption properties of Mg + 10wt.%X (X= V, Y, Zr) submicrocrystalline composites. Journal of Alloys and Compounds.
- Jan F. Rabek, (2002) Book of Experimental Methods in Polymer Chemistry,  
A Wiley Interscience Publication.
- A. Bettelheim, J. Hayon, S. Weiss, Z. Cherna, R. Ydgar, D. Ozer, (1998)  
Reflection – FTIR spectroelectrochemistry using ionically conductive polymer films: electrochemical preparation and spectroscopic characterization of some metal hydride.



### APPENDIX A: Mol & Mass Calculation for Alloy compounds.

Mol & mass calculation for  $\text{La}_{1-x}\text{Fe}_x\text{Mn}$ , ( $X = 0.05, 0.1, 0.2$ )

Molecular weight calculation:

$$\begin{aligned}\text{La}_2\text{O}_3 & \\ &= (139.91 \times 2) + (3 \times 16) \\ &= 327.82 \text{ g/mol}\end{aligned}$$

$$\begin{aligned}\text{Fe}_2\text{O}_3 & \\ &= (2 \times 55.45) + (3 \times 16) \\ &= 158.9 \text{ g/mol}\end{aligned}$$

$$\begin{aligned}\text{MnO}_2 & \\ &= 55 + (2 \times 16) \\ &= 87 \text{ g/mol}\end{aligned}$$

$$\begin{aligned}\text{Total molecular weight} &= (327.82 + 158.9 + 87) \text{ g/mol} \\ &= 573.72 \text{ g/mol}\end{aligned}$$

Basis of alloy is 10g

Mol for the alloy:

$$\begin{aligned}\text{Mol} &= m/\text{MW} \\ &= 10 \text{ g} / 573.72 \text{ g/mol} \\ &= 0.0174 \text{ mol}\end{aligned}$$

Calculate  $\text{La}_{1-x}\text{Fe}_x\text{Mn}$  when:

$$X = 0.05$$



$$\begin{aligned}\text{La}_{1-x} &= \text{La}_{1-0.05} = \text{La}_{0.95} \\ 0.95 \times 0.0174 \text{ mol} &= 0.0165 \text{ mol} \\ \text{Mass of La}_{0.95} &= 0.0165 \text{ mol} \times 327.82 \text{ g/mol} \\ &= 5.42 \text{ g}\end{aligned}$$

$$\begin{aligned}\text{Fe}_x &= \text{Fe}_{0.05} \\ 0.05 \times 0.0174 \text{ mol} &= 0.00087 \text{ mol}\end{aligned}$$

**APPENDIX B: Table for Hydrogenation data**

Alloy: X = .....

Initial Pressure: .....

Temperature: .....

Alloy mass (g): .....

**Table Appendix B: Table for Hydrogenation data**

x	Initial weight(g)	Final weight(g)	Weight loss(g)	Weight loss (%)
0.05				
0.1				
0.2				

## APPENDIX D: Tangent Line of TGA Curve

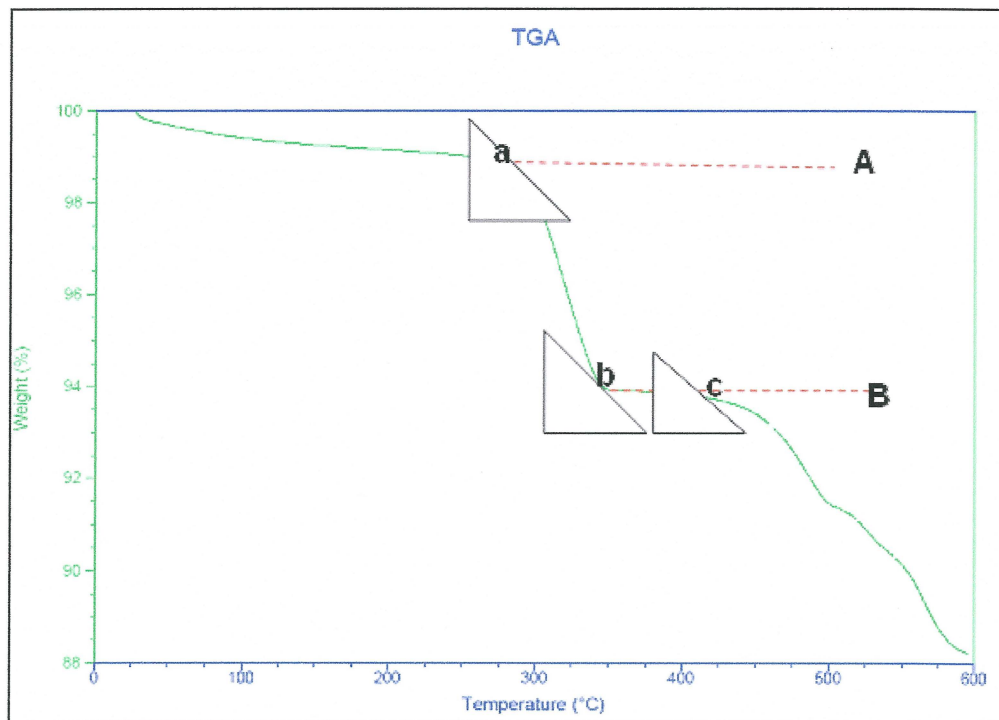


Figure 16 Tangent of TGA Curve.